**SUPPLEMENTARY INFORMATION**

# Gold nanorods-assisted theranostic solution for non-visible residual disease in bladder cancer

Paolo Armanetti, Irene Locatelli, Chiara Venegoni, Elisa Alchera, Beatrice Campanella, Filippo Pederzoli, Mirko Maturi, Erica Locatelli, Silvia Tortorella, Flavio Curnis, Angelo Corti, Roberta Lucianò, Massimo Onor, Francesca Sanvito, Andrea Salonia, Francesco Montorsi, Marco Moschini, Viktor Popov, Jithin Jose, Mauro Comes Franchini, Ean H Ooi, Luca Menichetti, Massimo Alfano.

## MATERIAL AND METHODS

**Histological analysis on the human patient cohort.** Clinical specimens collected through transurethral resection of bladder tumor (TURBT) were as follows: i) forty-three tissues with a diagnosis of high-grade NMIBC (CIS, n=25; pTaG3, n=11; pT1G3, N=7) and ii) four non-oncological bladder tissues with chronic reactive urothelium collected through re-TURB from the follow-up of four prostate cancer patients after radical prostatectomy and radiotherapy.

All surgical specimens encompassed the entire bladder wall and were staged according to the TNM classification and morphoarchitectural criteria according to the WHO classification (1, 2). Formalin-fixed paraffin-embedded blocks were retrieved and stained using an automatic hematoxylin/eosin (HE) slide stainer (HistoCore SPECTRA ST, Leica). An expert genitourinary pathologist reviewed the HE slides.

Immunohistochemistry was conducted on 2 µm tissue sections dewaxed in TE buffer for 40 minutes at 97 °C. After washing with TBS and quenching the endogenous peroxidase with 3% $H_2O_2$, tissue sections were incubated with 1/400 dilution of rabbit recombinant monoclonal integrin alpha 5 antibody (clone EPR7854, Abcam) for 1 h at room temperature. After washing, the binding of rabbit primary antibodies was detected using a Universal HRP-Polymer Biotin-free detection system (MACH4, BioCare Medical, USA) and 3,3-diaminobenzidine free base (DAB) as a chromogen. Tissue samples were then counterstained with Harris hematoxylin.

immunohistochemistry for the beta1 integrin was carried out as reported above by incubating tissue sections with 1/2000 dilution of rabbit recombinant monoclonal integrin beta 1 antibody (clone EPR16895, Abcam).

**Murine orthotopic bladder tumor model.** Orthotopic bladder tumors in mice developed after intravesical instillation of murine bioluminescent MB49-Luc bladder cancer cells, as recently reported (3). Briefly, female albino C57BL/6 J mice (9 weeks old, weighing about 20 g,

Charles River Laboratories, Italy) were anesthetized with ketamine (80 mg/kg) and xylazine (15 mg/kg) and kept in the dorsal position. Using a 24-gauge catheter, the bladder of each mouse was emptied and instilled with or without MB49-Luciferated (MB49-Luc) cells ($10^5$ cells/100 μl in DPBS). After 30 min, the catheter was removed, and the mice were returned to their cages for recovery. MB49-Luc cells were cultured in DMEM Glutamax medium (Gibco; Thermo Fisher Scientific) with standard supplements (1% penicillin/streptomycin and 10% FBS).

**Tumor growth monitoring.** Tumor growth was monitored by measuring the tumor volume using US imaging (see below) and in vivo optical imaging, such as bioluminescent quantification of MB49-Luc cells, after the administration of luciferin (15 mg/kg, intraperitoneal) using the non-invasive In Vivo Imaging System (IVIS, PerkinElmer, USA).

**Histological analysis on murine tissue.** Murine bladders were explanted, filled with 200 μl of 10% buffered formalin, placed in 10% buffered formalin for 24–48 hrs at room temperature, and then embedded in paraffin. Formalin-fixed paraffin-embedded consecutive sections (4 μm thick) were dewaxed and hydrated through a graded alcohol series, stained for histological analysis by bright-field microscopy, and stained using standard protocols for Hematoxylin and Eosin (Mayer's Hematoxylin, BioOptica #05-06002/L and Eosin, BioOptica #05-10002/L). Multiple sections from each sample were histologically evaluated, and the slides were acquired using Aperio AT2 digital scanner at 20x magnification (Leica Biosystems).

**Intravesical instillation of GNRs@Chit-Iso4.** GNRs synthesized for the present study have an average length of 90.2 ± 7.2 nm, an average width of 24.9 ± 2.6 nm, an aspect ratio of 3.62 ± 0.67, and a maximum absorption wavelength of 800 nm, and functionalized with the peptide

Iso4 (**Supplementary Figure S1**) as recently reported (3). GNRs@Chit-Iso4 was produced and instilled into the bladder through a catheter using a protocol similar to our previous study (3), with the only protocol modification being the infusion and aspiration of liquid into the bladder lumen to maintain the instilled GNRs in suspension, instead of ultrasound-mediated shaking. Liquid infusion and aspiration were performed three times during the 15 min incubation period.

**Protocol for in vivo GNR-assisted imaging and photothermal therapy of bladder cancer lesions.** The protocol for in vivo GNR-assisted imaging and photothermal therapy was designed and optimized according to the routine practice of TURBT. The protocol foresees six steps: i) urine removal and bladder wash out with saline solution, ii) intravesical instillation of urine stable GNRs specific for the recognition of the integrin α5β1 (GNR@Chit-Iso4, 100 μl of 100 μM solution), iii) suspension of the GNRs@Chit-Iso4 inside the bladder for 15 min by infusing and aspiring the liquid contained in the bladder with the catheter, iv) removal of the instilled solution and performing two intravesical washes with saline solution, v) visualization of the GNRs bound to the tumor by irradiating the top of the abdomen with 808 nm nano-pulsed laser, and vi) GNR-assisted PTT induced by 3 min irradiation with 808 nm continuous laser, with a calculated power density of 2.4 W/cm$^2$ on the skin. All steps were performed at room temperature.

**In vivo visualization of the GNRs@Chit-Iso4 bound to the tumor.** PA and US imaging were carried out on female albino C57BL/6 J mice bearing orthotopic bladder tumors following intravesical instillation of GNRs@Chit-Iso4. High-resolution US and PA imaging were performed using the Vevo LAZR-X platform (FUJIFILM VisualSonics, Inc.,Toronto, ON, Canada). The imaging platform included a high-frequency US system (Vevo 3100) combined

with an Nd:YAG nanosecond pulsed laser at a repetition rate of 20 Hz. The linear US transducer array Mx 550D consist of 256 elements with a nominal center frequency of 40 MHz (25–55 MHz bandwidth), a spatial resolution of 40 μm, and a maximum imaging depth of 15 mm. Light from the laser was delivered to the tissue through optical fibers mounted on either side of the transducer. Because GNRs are susceptible to morphological changes at higher laser threshold, light attenuators were used to reduce the laser fluence to avoid reshaping GNRs, as recently reported (3). During volumetric US-PA acquisition, a stepper motor was used for the linear translation of the US transducer and optical fibers along the sample. The linear stepper motor moves in steps of a minimum of 0.1 mm while capturing 2-D parallel images, for a maximum 3D range distance of 6.4 cm.

A 3D B-mode scan was performed on the mouse bladder. PA spectra between 680 and 970 nm were scanned with a step size of 5 nm in a single frame of the mouse bladder. For the in vivo studies (murine bladder), the 3D multispectral PA scans were acquired by selecting the PA spectral curve of tissue components, namely melanin, deoxy- and oxy-genated blood, and of the GNRs. The processed wavelengths (680, 722, 764, 810, 924, 970 nm) were automatically selected from the spectral curve used to spectrally unmix the GNRs signal from other endogenous tissue chromophore signals such as oxy- and deoxy-hemoglobin. The algorithm reported by Luke et al. was used to select these wavelengths, which is ideal for separating GNR signals from other endogenous absorbers (4). Data analyses were conducted using the Vevo®Lab software, and the volumes of interest were obtained by manually drawing the boxes on the 3D B-mode images. GNRs, melanin, and oxy- and deoxyhemoglobin contents were estimated from spectroscopic data using spectral unmixing analysis.

**In vitro photothermal therapy (PTT) of murine bladder cancer cell line MB49-Luc.** MB49-Luc cells were seeded at $5x10^3$ cells/well in 96-well plates and left untreated or treated

with 100 µM GNRs@Chit or GNRs@Chit-Iso4 for two hours. Cells were then washed twice with complete culture medium, irradiated with an 808 nm continuous laser at 3 W/cm$^2$ for 5 min, washed twice with complete culture medium, and suspended in 200 µl of complete culture medium. Cell viability was measured 16-hour later using the colorimetric assay WST-8 (Abcam).

**In vivo photothermal treatment**. The photothermal therapy (PTT) setup that was implemented comprises the following components: a continuous wavelength (CW) laser at 808 nm (CNI Lasers), an optical fiber (M59L02 1 mm Ø, 0.5 N.A., Thorlabs), and a power meter (sensor S405C, Thorlabs). The laser power, which was emitted from the optical fiber, was set to 0.66 W after being checked by the power meter. The tip of the optical fiber was placed 11 mm above the shaved skin of the mouse's abdomen. PTT was performed for 3 min.

**Measurement of temperature rise during GNR-assisted PTT.** To obtain an unbiased measurement of the temperature rise inside the bladder during GNR-assisted PTT, we isolated the bladder from the mice while keeping the skin and tissues between the skin and upper part of the bladder intact. We designed a specific setup using optomechanics components (Thorlabs) to create a "laser cage tower" with three levels: the upper level for aligning the optical fiber, the middle level for housing the sample, and the lower level for optical access of the near-infrared (NIR) thermal camera (**Supplementary Figure S3A-B**).

During the experiment, the mouse bladder (skin, peritoneum, bladder) was placed on the second level of the laser cage tower above a hole plate. Laser illumination was applied at the top. At the bottom of the laser cage tower, the NIR thermal camera recorded the temperature across the outer surface owing to thermal stimulation inside the bladder. Thermal acquisitions were performed for three different sets of mouse bladders: healthy bladders, bladders with

tumors, and bladders with tumors treated with GNRs@Chit-Iso4 (**Supplementary Figure S3C**). The characteristics of the laser and the irradiation duration were the same as those reported in "In vivo photothermal treatment."

**Measurement of the laser power density at the skin surface and bottom of the bladder.** To determine the power density of the laser light at the skin surface and the bottom surface of the bladder, characterization of laser irradiation used for photothermal therapy (PTT) was conducted on ex vivo mouse bladder tissue using a specially designed setup (**Supplementary Figure S5**). The beam and power distribution of the laser light were measured by positioning an optical fiber (M59L02, Thorlabs) perpendicular to the power meter sensor (Thorlabs s405c) that could be adjusted using a motorized linear stage (Zaber X-LHM) (**Supplementary Figure S5A-B**). The acquired data were post-processed and fitted with a fourth-degree polynomial function (**Supplementary Figure S5C**). We further evaluated the spatial infrared radiation (IRR) distribution and effective area of irradiation under the same geometrical conditions. The IRR distribution was fitted using a Gaussian distribution corresponding to the nature of the IRR source (**Supplementary Figure S5D**). The assessment of the power delivered to the bladder was based on the same geometrical constraints as those used during the thermal treatment in mice. A black target sensible to the laser IRR, placed 11 mm (the same distance used in vivo) from the fiber exit, was used to measure the actual angular aperture. The amount of incident power was calculated based on the integral average of the power-distribution curve within the range of the measured aperture angle.

Next, the power density was assessed in ex vivo mouse bladders (**Supplementary Figure S5E-G**). Power per unit area was quantified to assess power density within the bladder. The mouse bladder was harvested along with a related anatomical upper region that included skin and peritoneal fat, then placed on a power meter sensor and covered again with the resected tissue

region that was stretched to preserve the typical morphology **(Supplementary Figure S5E-G)**. Next, the optical fiber was placed at a height of 11 mm from the skin, after which laser irradiation was performed. The laser power measured at the bottom of the bladder surface was recorded and the power density was calculated with respect to the geometric shape and dimensions of the samples. The measured power density was corrected for transmittance (5) (**Supplementary Table S1**).

**Quantification of gold.** Inductively coupled plasma mass spectrometry (ICP-MS) was used to quantify gold in the bladder removed from either untreated animals or after intravesical instillation of GNRs@Chit-Iso4. The excised bladders were fixed in formalin, freeze-dried, and weighed. Then, 200 µl of aqua regia (3 ml of conc. HCl + 1 ml of conc. $HNO_3$), and 100 µl of 30% $H_2O_2$ were added directly into Eppendorf tubes containing the samples. The mixture was then heated for 2 h at 90°C. The samples were subsequently treated in an ultrasonic bath for 30 min without heating, and then centrifuged. Before the analysis, 100 µl of the supernatant was mixed with the eluent used for the flow-injection analysis (10 mM cysteine + 1% formic acid) to bring it to 1 ml. To quantitatively analyze the samples, a calibration curve was prepared by diluting 10 mg/l stock solution of Au in 0.05% HCl to concentrations of 10, 20, 50, and 100 µg/l in 10 mM cysteine + 1% formic acid. The analysis was carried out using ICP-MS by coupling a liquid chromatograph (1260 Infinity II LC Systems, Agilent) with a plasma mass spectrometer (Agilent 7700 ICP-MS) and injecting 50 µl of either the Au standard or sample. The 197Au isotope was used for quantification, and the signal at m/z 80 (relative to ArAr+) was monitored to evaluate the stability of the plasma (**Supplementary Figure S6**).

**Mathematical modelling of GNR-assisted photothermal therapy.** A coupled Monte Carlo finite element method was used to simulate the laser propagation and heat transfer processes

inside the tissue during the GNR-assisted PTT. A heat transfer model was developed by considering the thermal and optical properties of the murine bladder, surrounding tissue, tumor, and urine. The optical properties of the GNRs were derived using the Mie-Gans theory for a nanorod 24.9 nm in diameter and an aspect ratio of 3.62, as previously reported (6, 7). For the GNRs under investigation, the estimated peak absorption occurred at 811 nm, which is close to the experimentally determined 808 nm peak determined experimentally (3). The model accounts for the kinetics of heat release of GNRs@Chit-Iso4 when irradiated with a 0.66 W continuous laser. Heat dispersion by natural convection due to the movement of urine inside the bladder has also been considered (6-8).

**Quantification of heat absorption.** The heat absorbed by the tissue during GNR-assisted PTT can be estimated using Fourier's law: $Q/\Delta t = kA\Delta T/L$, where $k$ is the tissue thermal conductivity, $A$ is the cross-sectional area of the heat flow, $L$ is the distance or thickness of the tissue, $\Delta T$ is the difference in temperature across the tissue, $Q$ is the magnitude of the heat flow, and $\Delta t$ is the heat flow duration under consideration. Because the preclinical model of orthotopic bladder cancer uses syngeneic cancer cells, and by assuming that the area of heat flow and distance are identical in all experiments, the values of $k$, $A$ and $L$ can be assumed to be the same for all experimental conditions. Hence, the amount of heat absorbed during laser irradiation ($\Delta t$ = 3 min) and during the cooling phase ($\Delta t$ = 4 min) for different experiments can be compared by evaluating $(\Delta T) \times (\Delta t)$ and expressed in °C ·s.

**Computational modelling of tumor temperature rise.** To estimate the temperature increase inside the tumor, computational models that approximated the experiments conducted on the excised mouse bladder were developed. For simplicity, the bladder was assumed to be an ellipsoid with dimensions in the principal axes matching those of excised mouse bladders.

Bladder thickness was assumed to be uniform at 0.35 mm (9). The bladder was surrounded by a thin layer of tissue assumed to have a uniform thickness of 0.5 mm. This replicates the layer of skin and tissue surrounding the bladder that was excised together with the bladder (see "Measurement of temperature rise during GNR-assisted PTT"). The tumor was constructed by intersecting the ellipsoid representing the bladder with a smaller ellipsoid whose dimensions and position were varied by trial-and-error so that the surface of the tumor exposed to the lumen of the bladder matched closely (within 3% difference) to those in the experiments. This is shown in **Supplementary Figure S7**, while the values of the tumor surface area exposed to the bladder lumen for each of the five excised mouse bladders are presented in **Supplementary Table S2**. The requirement to match the surface area ensures that the amount of GNRs present across the tumor surface (**Supplementary Table S2**) is consistent between the experiments and the simulations. **Supplementary Figure S1A** illustrates the five models developed to represent five excised mouse bladders with varying tumor sizes.

The simulation provided two temperature values: the average temperature across the bottom half of the surrounding tissue surface (to match the temperature measured experimentally using a thermal camera), and the average surface temperature across the tumor surface exposed to the bladder lumen. The differences in the initial temperatures were evaluated for each bladder model.

**Inclusion & ethics statement.** All collaborators of this study have fulfilled the criteria for authorship required by PNAS journal have been included as authors, as their participation was essential for the design and implementation of the study. Roles and responsibilities were agreed among collaborators ahead of the research. This work includes findings that are locally relevant, which have been determined in collaboration with local partners. This research was not severely restricted or prohibited in the setting of the researchers, and does not result in

stigmatization, incrimination, discrimination or personal risk to participants. Local and regional research relevant to our study was taken into account in citations.

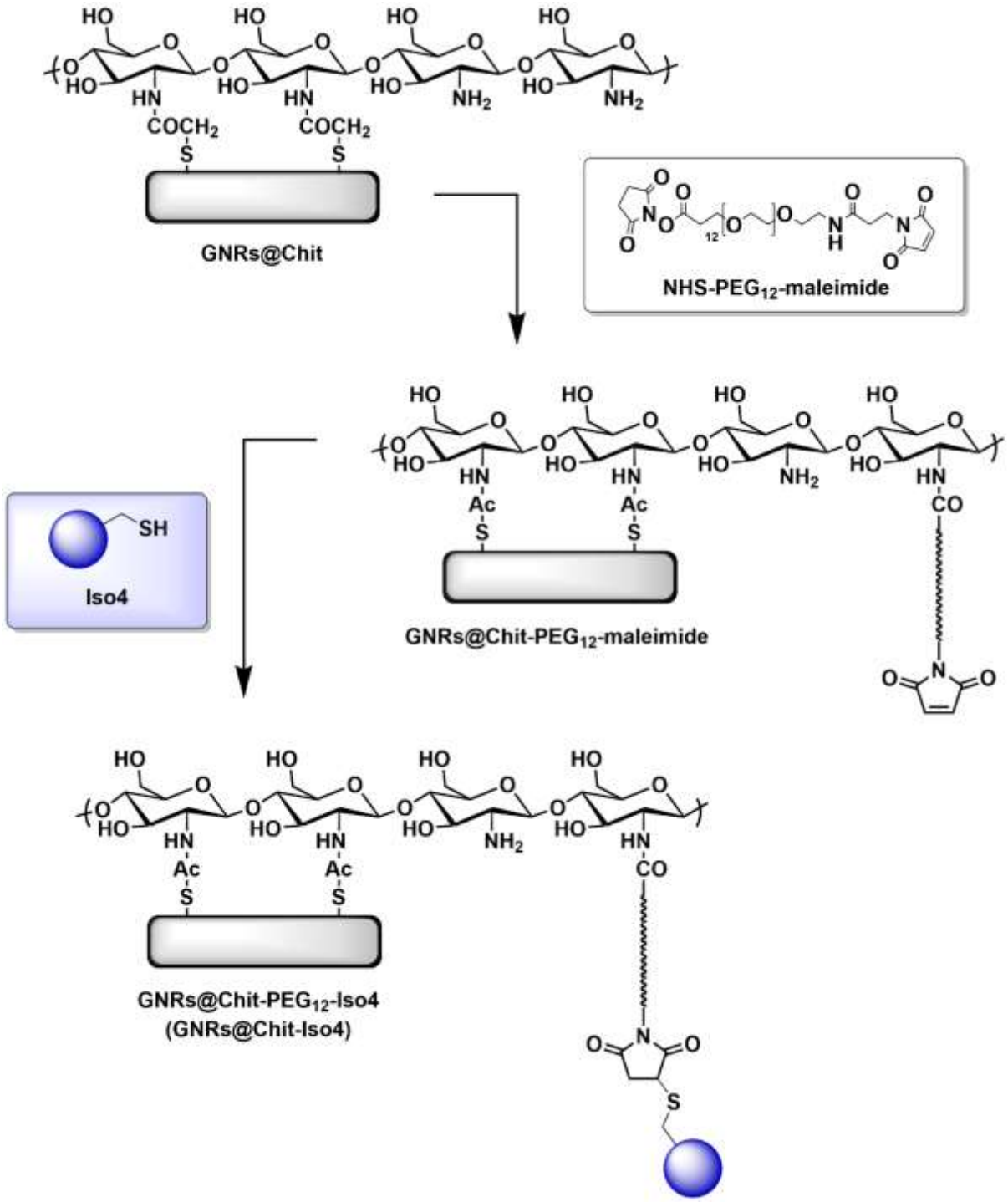


**Supplementary Figure S1. Schematic representation of the functionalization of chitosan-coated GNRs (GNRs@Chit) with Iso4 peptide.**

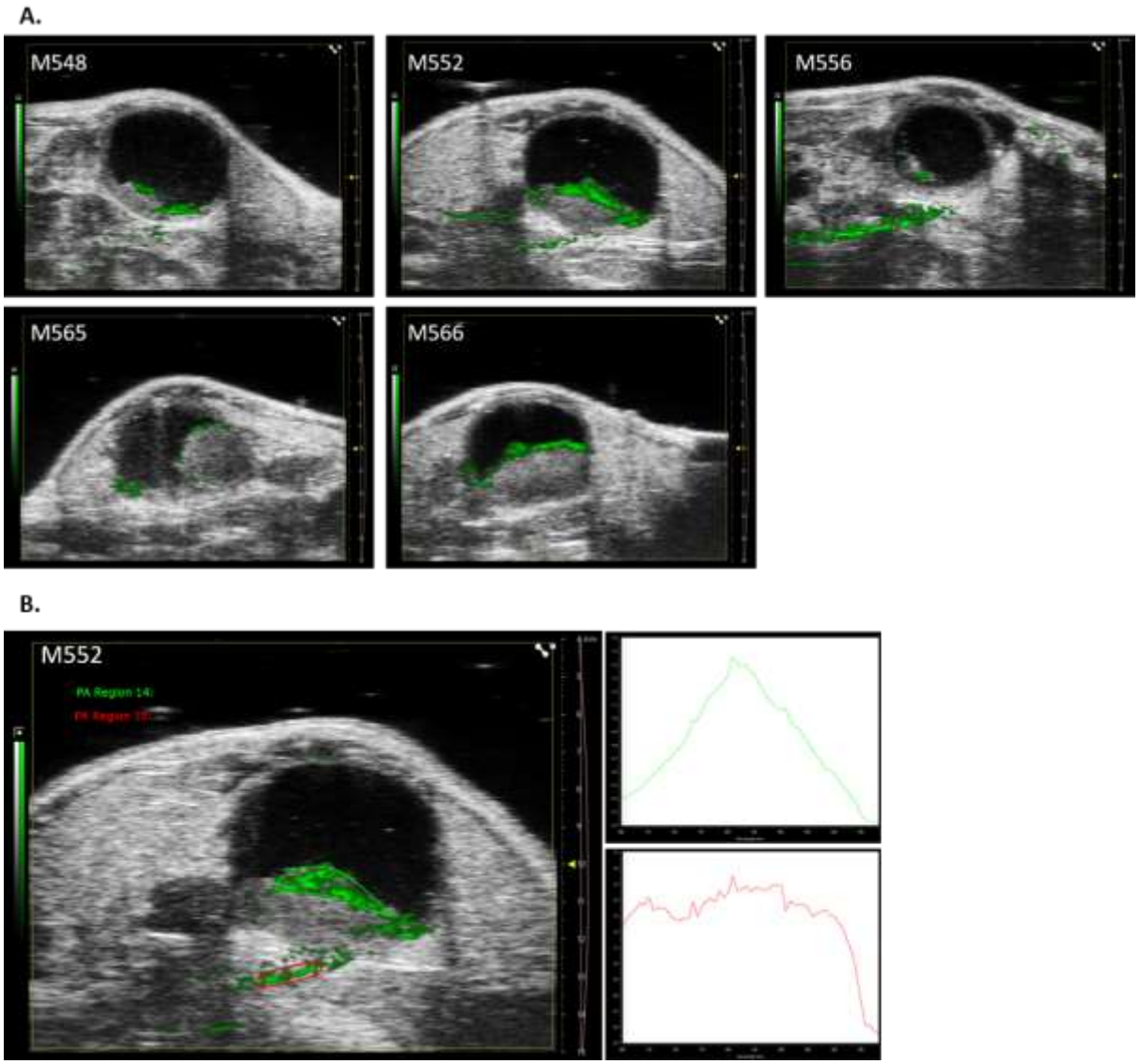


**Supplementary Figure S2. Multimodal imaging (photoacoustic and ultrasound imaging, PAUS) of murine orthotopic bladder cancer after intravesical instillation of GNRs@Chit-Iso4. A)** Representative PAUS images of the murine orthotopic bladder cancer 15 minutes after the intravesical instillation of GNRs@Chit-Iso4 (10 nmol Au) followed by 3 intravesical washes with saline solution; representative frame (axial frame, 2D) for each animal (n=5), with the orthotopic bladder cancer (US imaging) specifically recognized by GNRs@Chit-Iso4 visualized through PA imaging on the luminal area of the tumor (green signal). The TGC shown on the right side of each panel was identical for each acquisition. **B**) Representative image showing that the PA signal detected onto the luminal area of the tumor is from the

GNRs@Chit-Iso4 (PA spectra reported in the top panel), while unspecific PA signal was detected from the tissue surrounding the bladder (unspecific PA spectra reported in the bottom panel). The PA imaging of GNRs@Chit-Iso4 was obtained after unmixing the photoacoustic signal of melanin, deoxy- and oxy-genated blood acquired using the multiwavelength option.

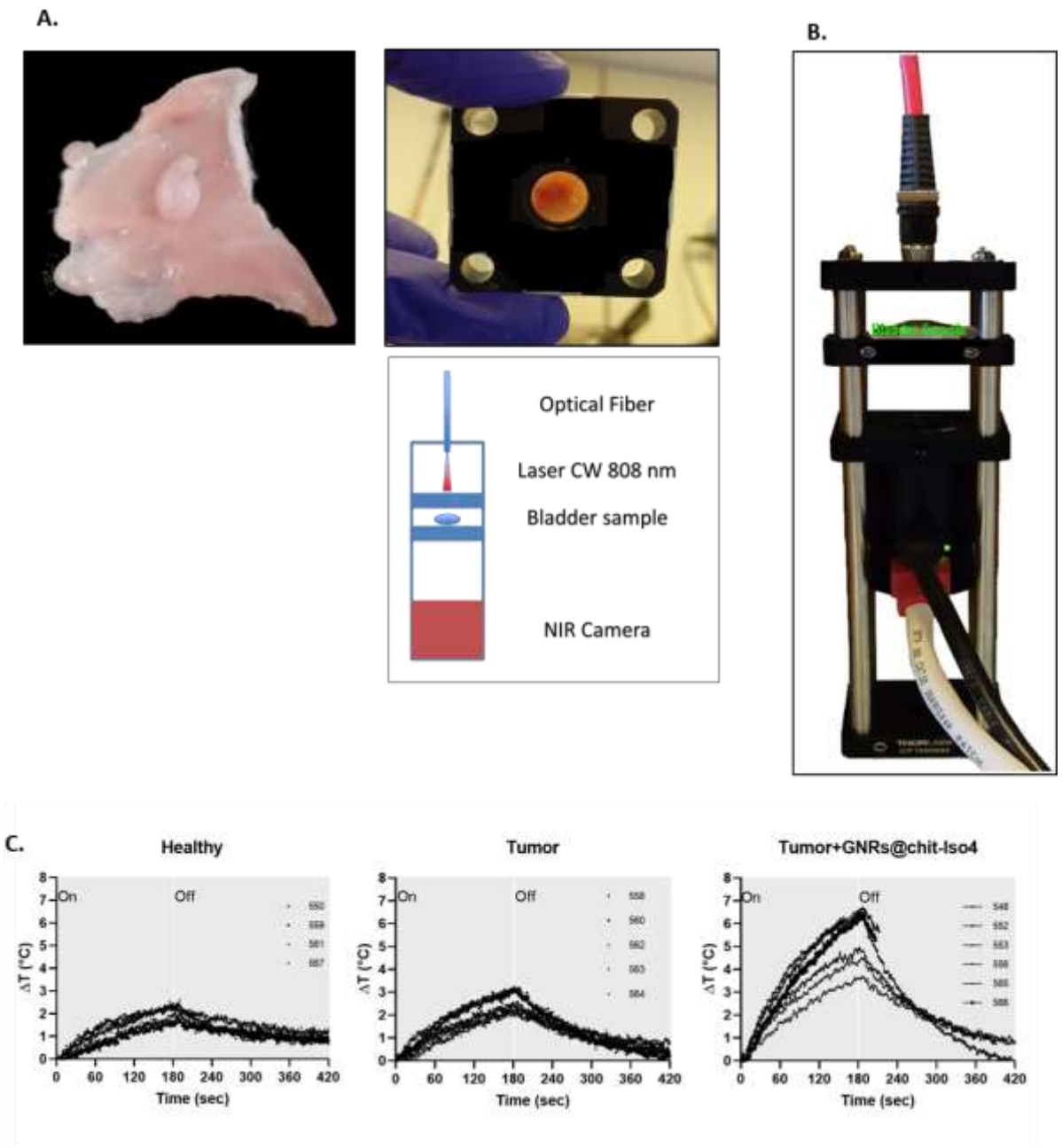


**Supplementary Figure S3. Setup for ex-vivo temperature measurement during laser irradiation of the explanted murine bladder. A**) From the animal in supine position the bladder from i) control animals, ii) animals with bladder cancer and iii) animal with bladder cancer and GNRs@Chit-Iso4 bound to the luminal side of the bladder (Supplementary Figure S1) were removed, keeping the skin and tissue between the skin and the bladder on the top of the bladder. The tissue was placed on a holder, which is part of a setup that includes the laser light on top and a near-infrared camera to measure the heat at the bottom. **B**) Picture of the

setup. **C**) Measurement of the delta of temperature (vs room temperature at 22 °C) during the heating (3 minutes) and cooling (4 minutes) periods for all tested conditions.

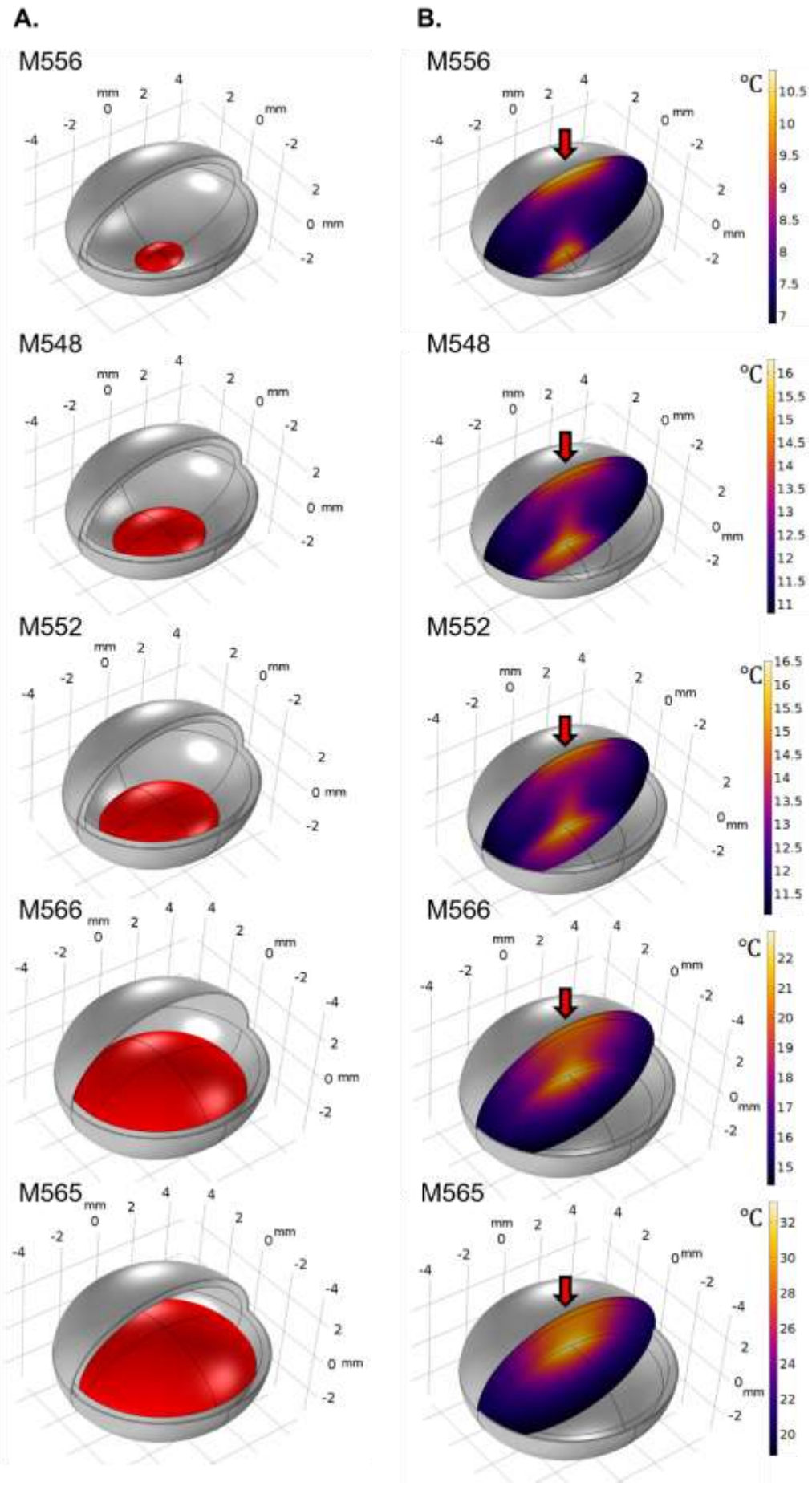
A.
B.
M556
M548
M552
M566
M565
°C
mm

**Supplementary Figure S4. Models developed to approximate the five excised mouse bladders and the simulated results. A**) The different models of the bladder and the surrounding tissue (both in gray) and the tumor (in red) corresponding to the different experimental cases. **B**) Distribution of temperature rise against the initial temperature across the sagittal plane of the bladder after 3 min of irradiation. The red arrow indicates the direction of laser irradiation. The contours have been plotted on independent scale for better visualization.

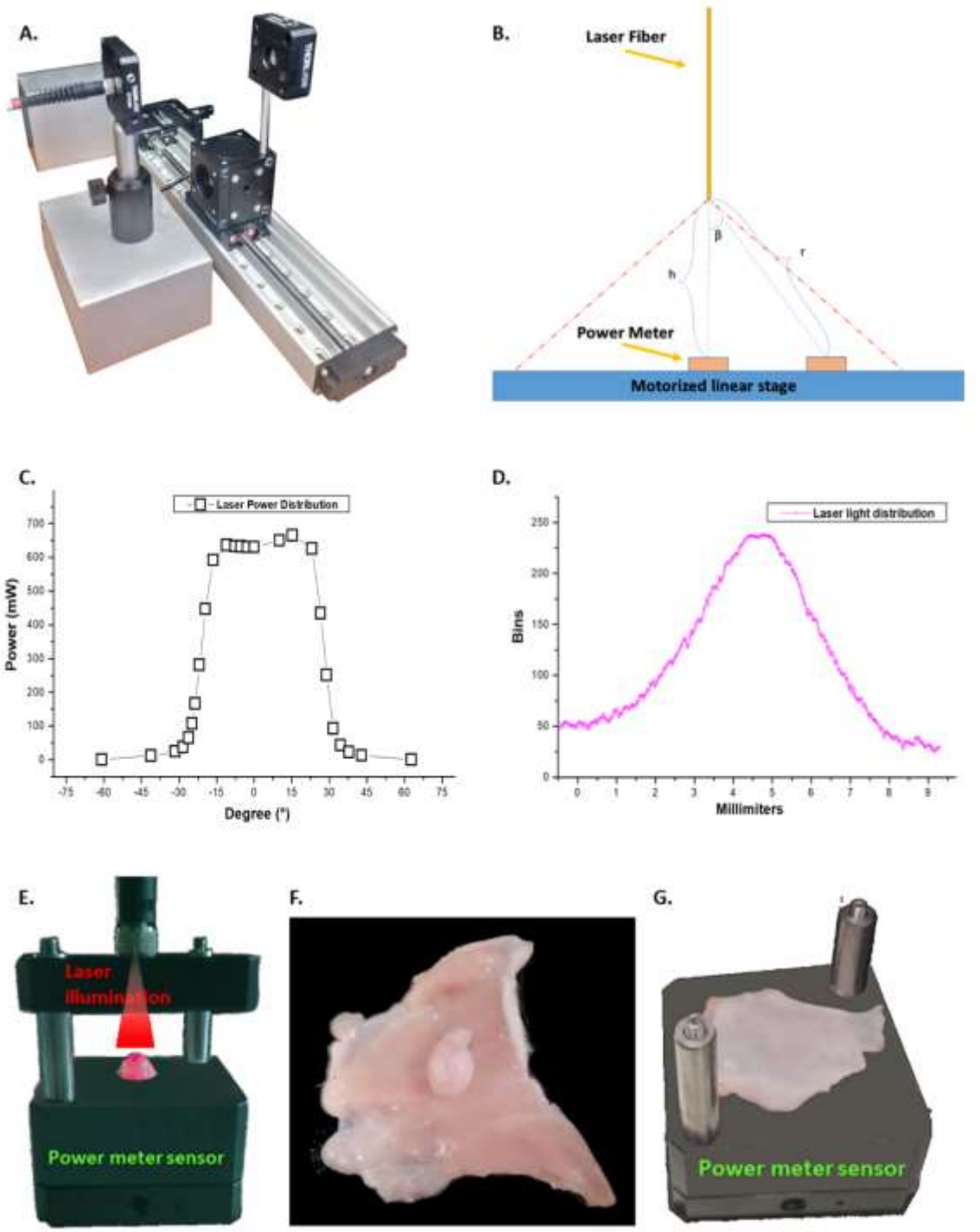


**Supplementary Figure S5. Technological setup for the measurement of laser illumination parameters. A**) The motorized linear stage used for positioning the optical fiber. **B**) Sketch of the optomechanical setup for the laser light and power distribution. **C**) Laser power angular distribution plot. **D**) Laser light distribution mean profile. **E**) The power meter sensor was

placed perpendicular to the optical fiber. **F**) The murine bladder was explanted, keeping it in contact with the skin covering the upper part of the organ, the skin was placed 11 mm from the laser beam, while the bottom part of the organ covered by the peritoneum was in contact with the power meter. **G**) The tissue is positioned to keep the same morphology as in the in-vivo conditions.

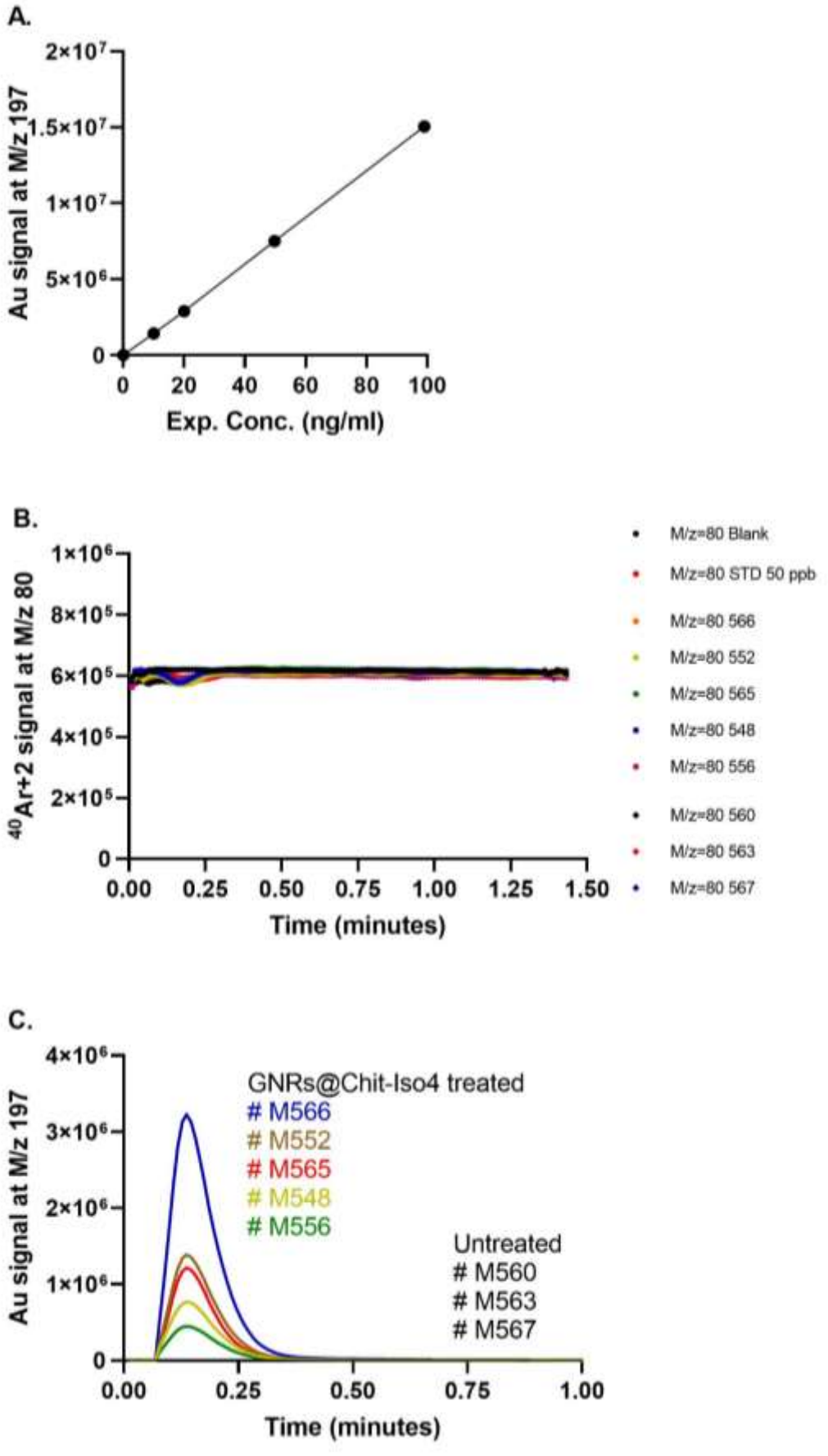
A.
Au signal at M/z 197
2×10^7
1.5×10^7
1×10^7
5×10^6
0
0
20
40
60
80
100
Exp. Conc. (ng/ml)
B.
40Ar+2 signal at M/z 80
1×10^6
8×10^5
6×10^5
4×10^5
2×10^5
0
0.00
0.25
0.50
0.75
1.00
1.25
1.50
Time (minutes)
M/z=80 Blank
M/z=80 STD 50 ppb
M/z=80 566
M/z=80 552
M/z=80 565
M/z=80 548
M/z=80 556
M/z=80 560
M/z=80 563
M/z=80 567
C.
Au signal at M/z 197
4×10^6
3×10^6
2×10^6
1×10^6
0
0.00
0.25
0.50
0.75
1.00
Time (minutes)
GNRs@Chit-Iso4 treated
# M566
# M552
# M565
# M548
# M556
Untreated
# M560
# M563
# M567

**Supplementary Figure S6. Gold quantification. A**) The ICP-MS was calibrated using $^{197}Au^{+}$ calibration curve in the range 0-100 µg/l. **B**) The plasma stability of ICP-MS system for $^{40}Ar^{+}_{2}$ signal at M/z 80 was assessed throughout the entire analysis session. **C**) Au signal at M/z 197 for the control samples (GNRs-untreated murine bladders, samples 560-563-567), and amounts of Au quantified into the GNRs-treated murine bladders.

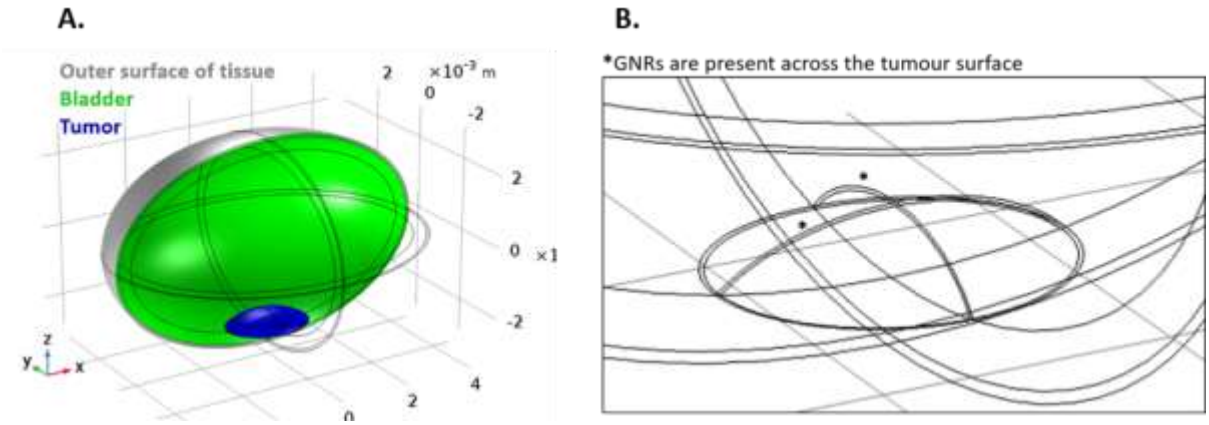


**Supplementary Figure S7. Model of the excised mouse bladder. A**) The 3D model used to simulate the geometry of the tumor and the distribution of the GNRs across the tumor surface: the tumor area and binding of the GNRs@Chit-Iso4 to the surface of the tumor of the five mouse tested were visualized by PAUS imaging (**Supplementary Figure S6**). **B**) The tumor surface measured through US imaging and obtained from the application of the computational model.

**Supplementary Table S1. Laser power density and energy on the skin surface and at the bottom of the bladder**.

| Acquisition | Laser source power (W) | Distance from the skin (cm) | Bladder dimension (w x d, cm) | Power density on the skin ($W/cm^2$) | Power density at the bottom of the bladder ($W/cm^2$) | Joule on the skin (J) | Joule at the bottom of the bladder (J) |
|---|---|---|---|---|---|---|---|
| **#1** | 0.660 | 0.11 | 0.5x0.5 | 2.54 | 0.802 | 118.69 | 113.38 |
| **#2** | 0.660 | 0.11 | 0.4x0.5 | 2.54 | 0.644 | 118.69 | 72.83 |
| **#3** | 0.660 | 0.11 | 0.6x0.4 | 2.54 | 0.600 | 118.69 | 81.43 |
| **#4** | 0.660 | 0.11 | 0.5x0.5 | 2.54 | 0.653 | 118.69 | 92.32 |
| **#5** | 0.660 | 0.11 | 0.5x0.5 | 2.54 | 0.702 | 118.69 | 99.24 |
| **#6** | 0.660 | 0.11 | 0.6x0.45 | 2.54 | 0.579 | 118.69 | 88.40 |
| **#7** | 0.660 | 0.11 | 0.5x0.4 | 2.54 | 0.630 | 118.69 | 71.25 |
| **#8** | 0.660 | 0.11 | 0.5x0.42 | 2.54 | 0.703 | 118.69 | 83.48 |
| **Mean±SEM** | | | | 2.54 | 0.664±0.070 | 118.69 | 87.79±13.95 |

Data from 8 independent experiments are presented. The laser power density ($W/cm^2$) and energy (J) were provided in 180 s of irradiation on the skin and at the bottom of the bladder wall.

**Supplementary Table S2. Quantification of gold bound to the surface of bladder cancer.**

| | **Bladder length (mm)** | **Bladder height (mm)** | **Bladder width (mm)** | **Bladder volume ($mm^3$)** | **Tumor area ($mm^2$)** | **Tumor volume ($mm^3$)** | **Au (ng)** |
|---|---|---|---|---|---|---|---|
| **Tumor+GNRs** | | | | | | | |
| M548 | 8.2 | 5.032 | 6.463 | 176.12 | 14.48 | 11.4 | 108.64 |
| M552 | 8.4 | 5.885 | 6.885 | 231.762 | 25.01 | 26.2 | 191.16 |
| M556 | 8.2 | 4.854 | 6.446 | 167.116 | 3.82 | 2.04 | 64.8 |
| 565 | 9 | 5.779 | 8.264 | 280.75 | 69.58 | 114.8 | 432.96 |
| 566 | 9 | 6.22 | 7.832 | 284.372 | 57.53 | 100.9 | 322.07 |
| **Tumor** | | | | | | | |
| M558 | 7.2 | 5.891 | 7.39 | 260.704 | 17.26 | 16.329 | |
| M560 | | | | 124.481 | 10.94 | 9.923 | |
| M562 | 6.6 | 4.522 | 6.036 | 183.809 | 7.67 | 5.418 | |
| M563 | 7.2 | 5.43 | 7.207 | 259.083 | 30.47 | 37.976 | |
| M564 | 7.6 | 6.312 | 8.146 | 166.977 | 13.4 | 9.867 | |
| | 8.2 | 4.356 | 6.915 | | | | |
| **Control** | | | | | | | |
| M559 | 8.4 | 4.862 | 8.058 | 231.731 | | | |
| M561 | 8.2 | 4.615 | 7.501 | 198.006 | | | |
| M567 | 8 | 4.743 | 7.861 | 214.601 | | | |
| M550 | 10.2 | 5.593 | 7.602 | 194.217 | | | |
| | 10 | 3.581 | 7.04 | | | | |

The length, height, width, volume, and area were measured from the scanned ultrasound image of the entire bladder. Quantification of gold (Au) was performed on explanted bladders fixed in formalin.

**Supplementary Table S3. Comparison of the measured tumor surface area exposed to the bladder lumen and that of the computational model.**

| **Case** | **Tumor area ($mm^2$)** | |
|---|---|---|
| | **Experiment** | **Model** |
| **M556** | 3.85 | 3.82 |
| **M548** | 14.25 | 14.48 |
| **M552** | 25.68 | 25.01 |
| **M566** | 57.61 | 57.56 |
| **M565** | 69.12 | 69.58 |

**Supplementary Table S4. Comparison of the measured temperature and numerical simulation to estimate temperature increase at top and bottom tumor surface.**

| **Experimental data** | | | | **Simulation with GNRs, ΔT (°C)** | | **Simulation without GNR, ΔT (°C)** | |
|---|---|---|---|---|---|---|---|
| **Case** | **Au (ng/mm$^2$)** | **Total Au (ng)** | **ΔT measured (°C)** | **Average top surface** | **Average bottom surface** | **Average top surface** | **Average bottom surface** |
| *__M556__ | 7.5 | 28.65 | 3.6 | 9.54 | 7.26 | 5.54 | 5.39 |
| **M548** | 7.5 | 108.64 | 4.94 | 13.91 | 11.53 | 5.81 | 5.62 |
| **M552** | 7.64 | 191.16 | 6.43 | 13.69 | 11.74 | 5.3 | 5.13 |
| **M566** | 5.6 | 322.07 | 6.2 | 17.36 | 14.81 | 6.39 | 5.97 |
| **M565** | 6.22 | 432.96 | 6.66 | 23.79 | 19.51 | 7.79 | 7.06 |

*Note that for M556, the total Au was estimated based on a density of 7.5 ng/mm$^2$ (i.e., the average) because the density was an outlier in the experiment.

## REFERENCES


1. M. J. Magers *et al.*, Staging of bladder cancer. *Histopathology* **74**, 112-134 (2019).
2. V. Tateo, V. Mollica, A. Rizzo, M. Santoni, F. Massari, Re: WHO Classification of Tumors, 5th Edition, Volume 8: Urinary and Male Genital Tumors. *Eur Urol* **84**, 348-349 (2023).
3. E. Alchera *et al.*, Early diagnosis of bladder cancer by photoacoustic imaging of tumor-targeted gold nanorods. *Photoacoustics* **28**, 100400 (2022).
4. G. P. Luke, S. Y. Nam, S. Y. Emelianov, Optical wavelength selection for improved spectroscopic photoacoustic imaging. *Photoacoustics* **1**, 36-42 (2013).
5. C. P. Sabino *et al.*, The optical properties of mouse skin in the visible and near infrared spectral regions. *J Photochem Photobiol B* **160**, 72-78 (2016).
6. E. H. Ooi, V. Popov, M. Alfano, J. K. K. Cheong, Influence of natural convection on gold nanorods-assisted photothermal treatment of bladder cancer in mice. *Int J Hyperthermia* **37**, 634-650 (2020).
7. J. K. Cheong *et al.*, A numerical study to investigate the effects of tumor position on the treatment of bladder cancer in mice using gold nanorods assisted photothermal ablation. *Comput Biol Med* **138**, 104881 (2021).
8. J. K. Cheong *et al.*, Gold nanorods assisted photothermal therapy of bladder cancer in mice: A computational study on the effects of gold nanorods distribution at the centre, periphery, and surface of bladder cancer. *Comput Methods Programs Biomed* **230**, 107363 (2023).
9. L. O. Leiria *et al.*, Functional, morphological and molecular characterization of bladder dysfunction in streptozotocin-induced diabetic mice: evidence of a role for L-type voltage-operated Ca2+ channels. *Br J Pharmacol* **163**, 1276-1288 (2011).